PHYSICAL REVIEW C **100**, 034601 (2019)

Measurement of the $^{10}\mathrm{B}(\alpha, n_0)\,^{13}\mathrm{N}$ cross section for $2.2 < E_\alpha < 4.9$ MeV and its application as a diagnostic at the National Ignition Facility

Q. Liu,[1] M. Febbraro,[2] R. J. deBoer,[1] A. Boeltzig,[1,*] Y. Chen,[1] C. Cerjan,[3] M. Couder,[1] B. Frentz,[1] J. Görres,[1] E. A. Henry,[3] E. Lamere,[1,†] K. T. Macon,[1,4] K. V. Manukyan,[1] L. Morales,[1] P. D. O'Malley,[1] S. D. Pain,[2] W. A. Peters,[2] D. Schneider,[3] C. Seymour,[1] G. Seymour,[1,‡] E. Temanson,[2] R. Toomey,[5] B. Vande Kolk,[1] J. Weaver,[6] and M. Wiescher[1]

[1]*Department of Physics, The Joint Institute for Nuclear Astrophysics, University of Notre Dame, Notre Dame, Indiana 46556, USA*
[2]*Oak Ridge National Laboratory, Oak Ridge, Tennessee 37830, USA*
[3]*Lawrence Livermore National Laboratory, Livermore, California 94550, USA*
[4]*Department of Physics and Astronomy, Louisiana State University, Baton Rouge, Louisiana 70803, USA*
[5]*Department of Physics and Astronomy, Rutgers University, New Brunswick, New Jersey 08901, USA*
[6]*Material Measurement Laboratory, National Institute of Standards and Technology, Gaithersburg, Maryland 20899, USA*

(Received 17 June 2019; published 3 September 2019)

The National Ignition Facility (NIF) provides the opportunity to study nuclear reactions under controlled conditions at high temperatures and pressures at a level never before achieved. However, the timescale of the deuterium-tritium (DT) implosion is only a few nanoseconds, making data collection and diagnostics very challenging. One method that has been proposed for obtaining additional information about the conditions of the implosion is to activate a dopant material using the α particles produced from the DT fuel as a diagnostic. The yield of the activated material can give a measure of the mixing that occurs in the capsule. One of the reactions that has been proposed is $^{10}\mathrm{B}(\alpha, n)\,^{13}\mathrm{N}$ as it produces a radioactive reactant product with a convenient half-life of $\approx$10 min. Although this reaction has several advantages for the application at hand, it has not seen much study in the present literature, resulting in large uncertainties in the cross section. Furthermore, for the current application, the cross section must be well characterized. With this motivation, the $^{10}\mathrm{B}(\alpha, n)\,^{13}\mathrm{N}$ cross section has been remeasured for $2.2 < E_\alpha < 4.9$ MeV with the angle-integrated ground-state cross section reported for the first time. The present results, combined with previous measurements, allow for a determination of the cross section to a significantly higher degree of accuracy and precision than obtained previously and are shown to be consistent with thick-target measurements. Preliminary calculations are performed to test the feasibility of this reaction as a diagnostic for a NIF implosion.

DOI: 10.1103/PhysRevC.100.034601

I. INTRODUCTION

The National Ignition Facility (NIF) [1] provides the opportunity to study matter under high-temperature and pressure conditions that are not currently achievable through any other means. These conditions are achieved by focusing 192 high powered lasers, delivering a total power of 500 TW to a target system and ultimately onto a single point a few millimeters in diameter. The conditions are comparable to those found in the heart of a star or at the epicenter of a nuclear detonation. In this environment, material is in the form of a plasma, whose physical properties remain poorly understood. NIF offers an experimental laboratory in which to study this environment first hand. Yet, the timescale of a NIF implosion (shot) is only a few nanoseconds, and the repetition rate is on the order of a few shots per day, making conventional measurements very challenging. Therefore, indirect and novel methods must be developed and utilized. For recent reviews of the high-energy-density physics at NIF see Hurricane and Herrmann [2] and Cerjan *et al.* [3].

One such indirect method for obtaining diagnostic information is activation, a longstanding technique in the nuclear physics community. NIF implosions often use equimolar deuterium-tritium (DT) as a fuel mixture, producing energy through the very exothermic (Q value of +17.6-MeV) $d(t, n)\alpha$ reaction. The reaction produces neutrons at $E_n \approx$ 14 MeV and α particles at $E_\alpha \approx 3.6$ MeV. These α particles are rapidly stopped in the high-density environment of the compressed capsule material [2] dumping additional energy into the system. This so-called α-boot-strapping effect is required to increase the energy budget towards ignition but has only been indirectly tested. Within the short range of the α particles, dictated by the stopping conditions, α-induced nuclear reactions can occur on fuel, ablater, and dopant materials in the capsule environment. These reactions can be utilized for testing the α-boot-strapping concept and to verify theoretical predictions of the phenomenon. Possible

---

[*] Present address: Gran Sasso National Laboratory, Via G. Acitelli 22, 67100 Assergi, Italy.

[†] Present address: Department of Physics and Applied Physics, University of Massachusetts Lowell, Lowell Massachusetts 01854, USA.

[‡] Present address: Rutgers University, Piscataway, New Jersey 08854, USA.

reactions in unprocessed fuel isotopes, such as ^{2}H$(\alpha,\gamma)\,^{6}$Li and ^{3}H$(\alpha,\gamma)\,^{7}$Li, may occur, but the low number of reaction products will remain unidentifiable compared to the natural lithium abundance in NIF materials. A good candidate for a dopant reaction is ^{10}B$(\alpha,n)\,^{13}$N because it produces a radioactive isotope that can be easily analyzed as a NIF product. The reaction product ^{13}N has a half-life of $t_{1/2} = 9.965(4)$ min [4]. This half-life is long enough that the ^{13}N material can be collected after the shot using the Livermore Radiochemical Analysis of Gaseous Samples (RAGS) system [5]. It is important to note that only reactions populating the ground state of ^{13}N will contribute to the final yield. This is because excited states of ^{13}N are proton unbound and will, instead, immediately decay to stable ^{12}C.

The total amount of ^{13}N that was produced in the shot will be measured, accounting for the measured collection efficiency of the RAGS system. The yield obtained in a NIF implosion is similar in some respects to the thick-target yield in accelerator-based experiments where the incoming beam is completely stopped in the target material [6,7]. To calculate the reaction yield, the ^{10}B$(\alpha,n_0)\,^{13}$N cross section must be integrated over the entire energy range below the initial α energy of $E_\alpha \approx 3.6$ MeV. Extensive studies have been performed to determine the stopping power in a laser plasma environment, but only limited experimental data are available about the cross section of the reaction, suggesting pronounced resonances over the entire low-energy range [8]. This paper concentrates on a more accurate determination of the cross section in order to calculate the thick-target yield for the NIF environment and to compare with previous accelerator-based thick-target experiments.

The ^{10}B$(\alpha,n)\,^{13}$N reaction was one of the first nuclear reactions studied that itself produces a radioactive product [9], and α-induced reactions on boron were used to make early measurements of the mass of the neutron [10,11]. Early measurements of the cross section were hindered as only radioactive α emitters were available to induce the reaction. The first accelerator-based measurement was by Bonner *et al.* [12], but they were unable to clearly disentangle contributions for the ^{10}B$(\alpha,n)\,^{13}$N and ^{11}B$(\alpha,n)\,^{14}$N reactions as the detection system was only sensitive to the number of emitted neutrons. This is a significant issue because the ^{11}B$(\alpha,n)\,^{14}$N reaction is approximately an order of magnitude larger than that of the ^{10}B$(\alpha,n)\,^{13}$N cross section over the energy range of interest [13]. Furthermore, the moderated proportional counter used for that study could not distinguish between the different neutron channels, making the conversion of their reaction yields into cross sections impossible. A later study by Gibbons and Macklin [14] was able to more clearly obtain yields for the ^{10}B$(\alpha,n)\,^{13}$N reaction but still used a moderating countertype detector (carbon sphere) that could not separate the different neutron channels. Van der Zwan and Geiger [8] then used stilbene scintillators to investigate the reaction. These detectors could separate the different neutron groups using spectrum unfolding, but measurements were, for the most part, limited to three angles ($\theta_{\mathrm{lab}} = 0$, 90, and 160°). Because of the complicated angular distributions of the reaction products, total cross sections could only be calculated at a few energies where additional measurements were made. More recently, Prior *et al.* [15] have again made measurements using a proportional counter setup. With the aid of detector modeling using MCNP and the approximate branching ratio information of Van der Zwan and Geiger [8], a better determination of the total cross section could be obtained between $E_\alpha = 2.2$ and 4.9 MeV.

In this paper, an experimental technique similar to that of Van der Zwan and Geiger [8] is utilized, except that detailed angular distributions are extended to the entire energy range of interest allowing for a determination of the angle-integrated cross section of the ^{10}B$(\alpha,n_0)\,^{13}$N reaction for $1.5 < E_\alpha < 5.0$ MeV. The present measurements utilize deuterated liquid scintillators. Like the stilbene detectors of Van der Zwan and Geiger [8], they are sensitive to the neutron energy by analyzing the recoil energy given by the scintillation light spectrum. Deuterium has been found to be preferable over hydrogen-based liquid scintillators because the light response spectrum presents a peaking at the highest recoil energy improving the condition of the detector response used in spectrum unfolding [16,17]. Using this method, the ^{10}B$(\alpha,n_0)\,^{13}$N cross section can be measured, which is the component needed for the determination of ^{13}N production from a NIF implosion.

First, the experimental setup is described in Sec. II, which is followed by a description of the spectrum unfolding technique used to extract the experimental yields in Sec. III. The determination of the cross section is described in Sec. IV, and then comparisons to thick-target yield measurements are made in Sec. V. Simulations of the reaction under NIF conditions are discussed in Sec. VI with concluding remarks given in Sec. VII.

II. EXPERIMENTAL SETUP

Measurements were performed at the University of Notre Dame Nuclear Science Laboratory. The ^{10}B$(\alpha,n)\,^{13}$N reaction was studied for α-particle beam energies ranging from $E_\alpha = 2.2$ to 4.9 MeV using the Stable Beam Accelerator for Nuclear Astrophysics 5-MV accelerator. Beam intensities between 0.1 and $20\,e\,\mu$A were impinged on the target. The detection system consisted of five deuterated liquid scintillator detectors, one of type EJ-301D [18] (size: 7.6-cm-thick × 7.6-cm diameter), one of type EJ-315 [16] (size: 7.6-cm-thick × 5.8-cm diameter), and three of type EJ-315M (size: 7.6-cm-thick × 5.8-cm diameter), and one high-purity germanium (HPGe) detector with an efficiency of 54% relative to a 3″ × 3″ NaI detector. The setup is shown in Fig. 1. As a reference detector, the EJ-315 was fixed 60(1)° at a distance (front face to target center) of 27(1) cm. The angular distribution measurements were made with the other four detectors, which were placed 63(1) cm from the target position and rotated on a swing arm to 12 angular positions covering an angular range of $20 < \theta_{\mathrm{lab}} < 150°$ in the laboratory reference frame. The HPGe was used to monitor secondary γ rays for the ^{10}B$(\alpha,p'\gamma)\,^{13}$C reaction and was placed at $\theta_{\mathrm{lab}} = 130°$ at a distance of 22.5(5) cm. The secondary γ ray yields were used to aid in troubleshooting during the experiment.

Target properties

Targets were prepared by electron-gun sputtering a thin layer of enriched [96.2(5)%] ^{10}B powder onto a 0.5-mm-thick

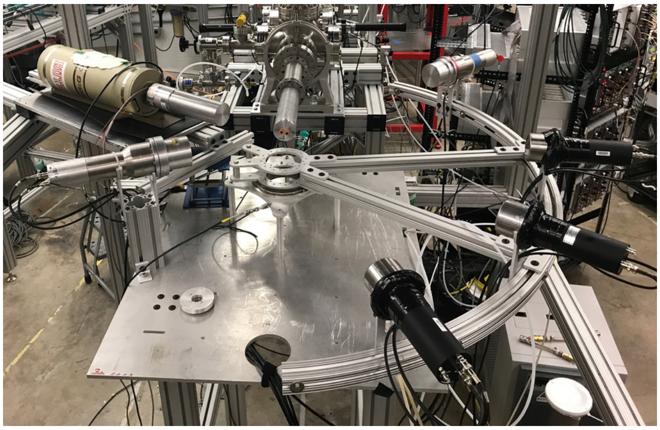

FIG. 1. Experimental setup. Positioned counterclockwise for the beam pipe are the HPGe, the EJ-315, the three EJ-315Ms, and the EJ-301D. The three EJ-315Ms and the EJ-301D are positioned on a swing arm to allow for additional angular distribution measurements.

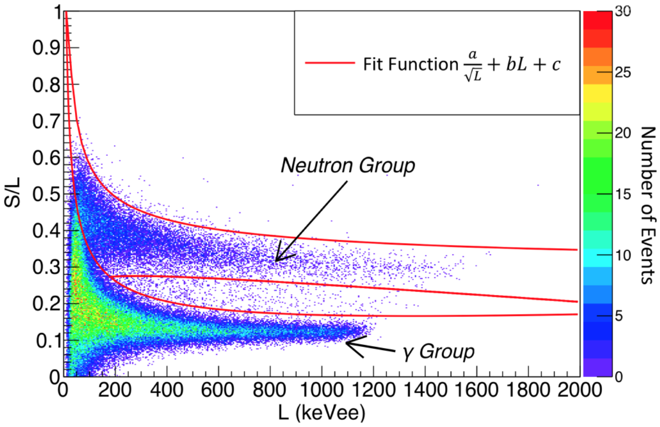

FIG. 2. Pulse shape discrimination plot for γ rays and neutrons for an EJ301D deuterated liquid scintillator. The vertical axis represents the ratio of the tail pulse integral (S) to the total pulse integral (L).

tantalum backing. The thickness and uniformity of the target was measured at the National Institute for Standards and Technology (NIST) Center for Neutron Research using cold neutron depth profiling with the neutron standard ^{10}B(n, α) ^{7}Li reaction [19,20]. Nine points, six with 3-mm diameter and three with 5-mm diameter, were measured across the target surface in order to gauge its homogeneity where the individual measurements had an uncertainty of less than 1%. These measurements revealed that the target varied in thickness by $\pm 10\%$ with a mean value of $13(1)\,\mu\text{g/cm}^2$. Because of the variation in the position of the beam spot on the target, the effective target thickness could not be determined to better than this level of accuracy. See Sec. IV for further discussion and the Supplemental Material [21] for a detailed description of the target characterization performed at NIST.

III. SPECTRUM ANALYSIS

Deuterated liquid scintillation detectors provide an alternative to time of flight for measuring partial neutron producing cross sections. The practical advantages include more flexibility in detector position from the target and no need for the pulsed beam. The former often results in higher geometric efficiency, and the latter often results in higher beam intensities. For this approach, the detector response must be carefully calibrated from the detector threshold up to the highest possible neutron energy incident on the detector in order to unfold the neutron energy spectrum accurately. The detectors described here have a neutron energy resolution of about 0.5 MeV and a low-energy threshold of about 1.3 MeV. The low-energy threshold is imposed by the limit on detector pulse shape discrimination (PSD) between neutrons and γ rays. An example two-dimensional PSD spectrum showing the tail integral divided by the total integral versus the total integral is shown in Fig. 2. The boundaries of the gates on the regions that are dominated by neutron and γ-ray events are motivated by the function $a/\sqrt{L} + bL + c$, where a, b, and c are adjustable phenomenological fit parameters and L is the total pulse integral. In the present analysis, the time windows for the pulse integrals have been defined relative to the 50% maximum k on the front edge of the pulse. The long integral is defined as the range from $(k - 25)$ to $(k + 175)$ ns, and the tail integral is defined as the range from $(k + 10)$ to $(k + 175)$ ns.

The ^{10}B(α, n_0) ^{13}N reaction at low energies is well suited for study using deuterated liquid scintillator detectors. The positive Q value of 1.058 73(27) MeV [22,23], the lowest beam energy studied ($E_\alpha \approx 2.5$ MeV), and the most backward angle of observation 150° give a lowest neutron energy of $E_n \approx 2.0$ MeV, well above the detector threshold limit. Furthermore, the first excited state of ^{13}N is at $E_x = 2.3649(6)$ MeV [4], allowing neutrons for the ground-state transition to be easily resolved from those populating the excited states. In addition, the ^{11}B(α, n) ^{14}N reaction is also energetically possible. Even with the small amount of ^{11}B ($< 4\%$) in the target, the larger cross section results in a similar yield. However, since the Q value of the ^{11}B(α, n) ^{14}N reaction is $Q = 0.157\,89(1)$ MeV [22,23], the neutrons from this reaction can be clearly separated from those of the ^{11}B(α, n_0) ^{13}N reaction.

The detector response has been calibrated against the well-known thick-target spectrum of the ^{9}Be(d, n) reaction over an energy range that spans those of the present measurements [24]. These calibration measurements were performed at the Edwards Accelerator Laboratory at Ohio University [25]. The detector response was modeled using MCNP-POLIMI [26]. As shown in Fig. 3, the simulation is able produce a satisfactory reproduction of the measured efficiency.

In order to extract yields for the individual neutron groups, it was necessary to unfold the neutron energy spectra. The spectrum unfolding technique used here has been benchmarked through a series of recent studies by Febbraro *et al.* [16] where a maximum-likelihood expectation maximization method has been utilized [27]. A typical unfolded spectrum is shown in Fig. 4 that can be compared directly to the spectrum obtained using stilbene detectors in Fig. 1 of Van der Zwan and Geiger [8]. The measured light output spectrum is represented in the bottom panel of Fig. 4 by the red line. The neutron detector's response matrix is calibrated using

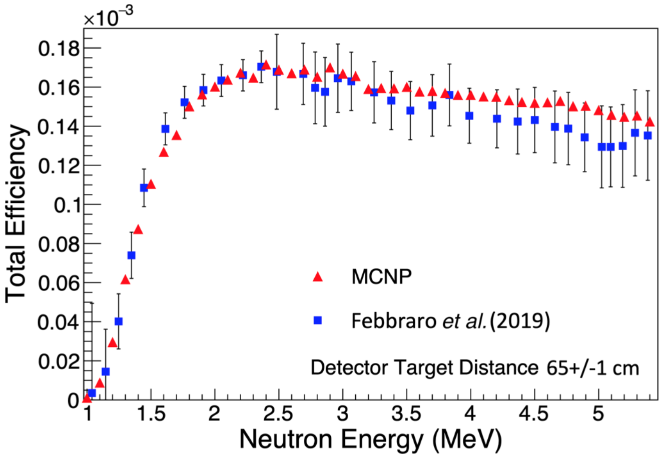

FIG. 3. Comparison of the efficiency curve of a 7.6-cm-thick × 5.8-cm-diameter EJ-315M deuterated liquid scintillator from a simulation using MCNP-POLIMI (red triangles) and the efficiency curve measured using time of flight with the ^{9}Be(d, n)-thick target method [24,25] (blue squares).

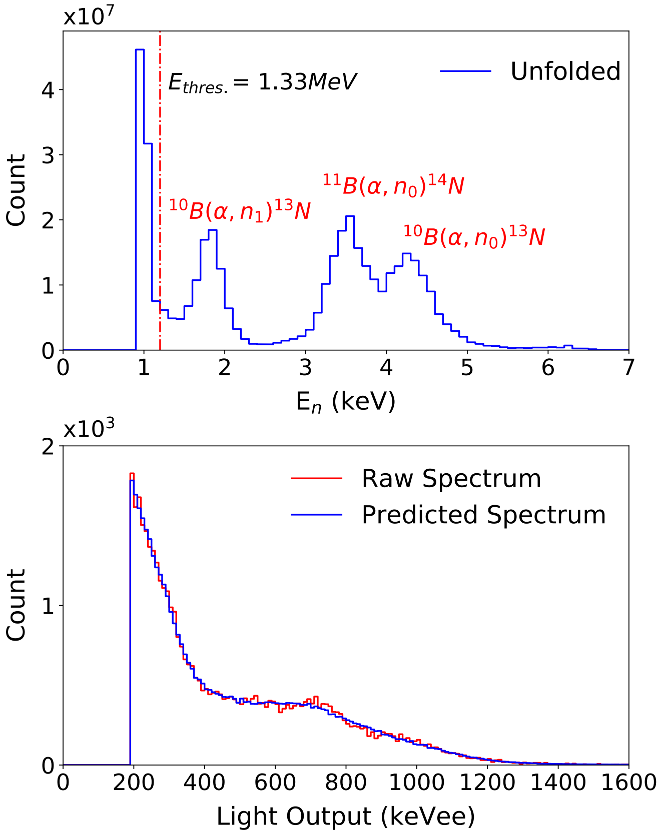

FIG. 4. Example of spectrum unfolding for a measurement at $E_\alpha = 4.84$ MeV and $\theta_{\mathrm{lab}} = 90^\circ$. The top panel shows the resulting unfolded neutron energy spectrum, which is unfolded using the well-calibrated detector response model. The bottom panel shows the raw light output spectrum (red line) compared to the resulting neutron spectrum in the top panel folded with the detector response (blue line).

time of flight and the ^{9}Be(d, n) reaction, and the detector response is modeled using MCNP-POLIMI. The blue line in the bottom panel represents a comparison of the extracted neutron spectrum folded with the detector response. In the top panel of Fig. 4, the individual neutron peaks appear that result from the unfolding of the measured light output spectrum. A threshold of $E_n = 1.33$ MeV is imposed based on the PSD threshold limitations shown in Fig. 2. Neutron emission populating the ground state and first excited state are clearly observed for the ^{10}B(α, n) ^{13}N reaction as well as the decay to the ground state in the ^{11}B(α, n) ^{14}N reaction.

IV. CROSS-SECTION DETERMINATION

As discussed in Sec. II, the effective target thickness was found to vary by up to ±10%. Therefore, to obtain a more accurate absolute cross section, the present angular distributions were normalized to the differential cross-section measurements of Van der Zwan and Geiger [8] at the common angle of 90° where the expected variation is ≈5%. As the angular distributions were measured with a fixed monitor detector (see Sec. II), they could be determined to a relative accurately of ≈ 10%. As the cross section varies slowly with energy compared to the energy losses through the target (10–17 keV), no target effect corrections were applied to the measured yields, and the beam energy is given as the energy of measurement.

A comparison of the present angular distribution measurement at $E_\alpha = 4.63$ MeV is made to that of Van der Zwan and Geiger [8] in Fig. 5. This is one of the few energies where Van der Zwan and Geiger [8] made measurements at several additional angles, providing a good comparison with the present measurements. Over the remainder of the region of interest, Van der Zwan and Geiger [8] made extensive measurements as a function of energy but only at three angles. The complicated angular distributions that they observed at a few sample energies indicated that sampling at three angles was insufficient for an accurate determination of the angle-integrated cross section in that work. The present measurements thus expand

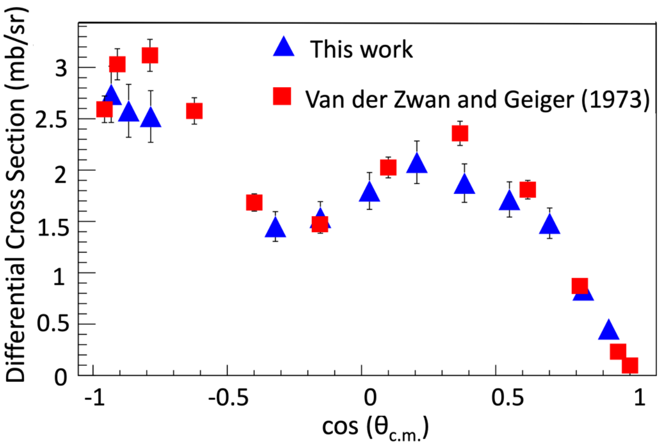

FIG. 5. Comparison of the angular distribution measurements at $E_\alpha = 4.63$ MeV from the present measurement (blue triangles) with those of Van der Zwan and Geiger [8] (red squares). Only statistical uncertainties are shown.

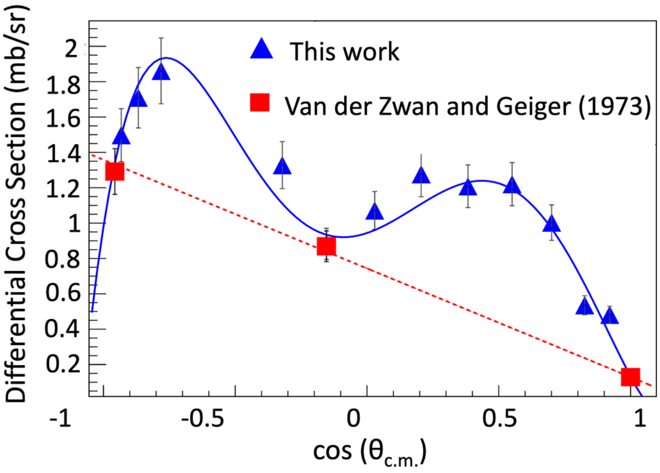

FIG. 6. Comparison of Legendre polynomial fits to angular distributions from the present paper (blue triangles) to that of Van der Zwan and Geiger [8] (red squares) at $E_\alpha = 4.768$ MeV. The present measurements at 12 angles reveal a significantly more complex angular distribution than inferred from the three angle measurements of Van der Zwan and Geiger [8]. To illustrate, a first-order Legendre polynomial (dotted red line) is sufficient to fit the angular distribution of Van der Zwan and Geiger [8], whereas a fifth-order Legendre polynomial (blue solid line) is required to match the present data.

on the work of Van der Zwan and Geiger [8] by sampling 12-point angular distributions at 34 energies between 2.2 and 4.9 MeV, allowing the angle-integrated cross section to now be mapped over the full energy range of interest. Figure 6 illustrates the complexity of the angular distributions and the need for these additional measurements. The differential cross sections for this paper after normalization to the 90° data of Van der Zwan and Geiger [8] are given in Table I.

To determine the angle-integrated cross section for the ^{10}B(α, n_0)^{13}N reaction, the differential cross sections were fit with a Legendre polynomial expansion in the center-of-mass reference frame. The order of the polynomial fit was determined by χ^2 statistics tests. The differential cross section can be written as a partial-wave expansion of the general form

$$\frac{d\sigma}{d\Omega}(\theta_{\text{c.m.}}) = \sum_{L=0}^{L_{\max}} a_L P_L \cos(\theta_{\text{c.m.}}), \qquad (1)$$

where the parameters a_L were determined by performing a χ^2 fit to the experimental data at each energy and $L_{\max}$, the highest-order Legendre polynomial of the fit, was determined using a p-value test. As in Van der Zwan and Geiger [8], the measured differential cross sections were observed to be both strongly varying with the angle and highly asymmetric about $\theta_{\text{c.m.}} = 90^\circ$ in the center-of-mass frame of reference. This indicates strong interference between broad overlapping resonances, which is reflected in the large odd-order angular distribution coefficients from the Legendre polynomial fits. Legendre polynomials of up to order $L = 5$ were necessary to describe some of the higher-energy angular distributions, which is consistent with the previous findings of Van der Zwan and Geiger [8]. The angular distribution coefficients are given in Table II where the angle-integrated cross section has been calculated as $\sigma = 4\pi a_0$.

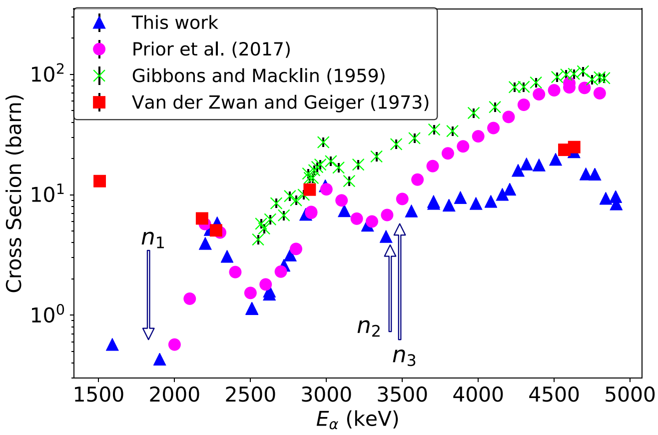

FIG. 7. Comparison of the ^{10}B(α, n)^{13}N angle-integrated cross-section measurements. Those of Gibbons and Macklin [14] (green stars) and Prior *et al.* [15] (pink circles) are total cross-section measurements (sum over all neutron deexcitations), whereas the present data (blue triangles) and those of Van der Zwan and Geiger [8] (red squares) are of the ground-state transition. The data of Gibbons and Macklin [14] show a large deviation from both the present measurements and those of Prior *et al.* [15]. The uncertainties in the present angle-integrated cross sections are estimated to be ≈6% as described in the text and are usually smaller than the points on the plot.

For the angle-integrated cross sections, the significant sources of uncertainty are from the Legendre polynomial fit (≈3%) and the normalization to the differential data of Van der Zwan and Geiger [8] (≈5% statistical, ≈15% systematic). In Van der Zwan and Geiger [8], the statistical uncertainties are not explicitly given but are quoted as being indicated by "the scatter of the measured points." From Fig. 2 of Van der Zwan and Geiger [8], over the relatively flat cross section around $E_\alpha \approx 3.75$ MeV, the statistical uncertainty is estimated to be ≈5%, which is also similar to the uncertainties that are given explicitly in Fig. 6 for the angular distributions of that work.

Measurements were made considering the previous data of Van der Zwan and Geiger [8] where excitation curves were mapped at three angles in very small energy steps. These data indicate a cross section that is dominated by resonances with widths of a few hundred keV. Therefore, the present measurements have been made with larger energy steps than that of Van der Zwan and Geiger [8] but still with a sufficient number to map the resonance structures. A cubic spline interpolation was then performed for each of the angular distribution coefficients at each measured energy in order to obtain the cross section at an arbitrary energy throughout the region. The interpolation was used for the numerical integration of the cross section to compare with thick-target yields as will be described in Sec. V.

A comparison to the data of Gibbons and Macklin [14] and Prior *et al.* [15] is shown in Fig. 7. The comparison is not one to one because the data of Gibbons and Macklin [14] and Prior *et al.* [15] are total cross-section

TABLE I. Differential cross sections in the laboratory frame of reference for the $^{10}\mathrm{B}(\alpha,n)^{13}\mathrm{N}$ reaction. The energies are those of the incident beam energy (E_α). Uncertainties in the α-particle beam energies are 3.0 keV. The tabulated uncertainties reflect the unfolding uncertainty, which is estimated to be ≈10%. The present data have a systematic uncertainty for measurements at different energies of ≈20%, therefore, they have been normalized to the data of Van der Zwan and Geiger [8] as described in the text.

	$d\sigma/d\Omega$ (μb/sr)											
E_α (keV)	20°	30°	40°	50°	60°	70°	80°	90°	100°	135°	145°	155°
1590	15(2)	34(3)	46(5)	55(5)	61(6)	65(6)	64(6)	64(6)	55(5)			
1902	25(2)	26(3)	28(3)	28(3)	28(3)	36(4)	35(3)	39(4)	38(4)	35(3)		
2202	170(17)	220(22)	251(25)	299(30)	332(33)	357(36)	388(39)	376(38)	354(35)	320(32)		232(23)
2235	334(33)	396(40)	401(40)	391(39)	406(41)	472(47)	439(44)	392(39)	433(43)	374(37)	376(38)	468(47)
2281	458(46)	511(51)	529(53)	495(49)	529(53)	576(58)	523(52)	505(50)	504(50)	355(36)	372(37)	
2346	300(30)	282(28)	318(32)	295(30)	301(30)	314(31)	290(29)	273(27)	252(25)	187(19)	167(17)	154(15)
2509	133(13)	134(13)	131(13)	138(14)	132(13)	120(12)	118(12)	93(9)	70(7)		43(4)	34(3)
2510	111(11)	141(14)	138(14)	139(14)	134(13)	123(12)	106(11)	94(9)	73(7)	45(5)	39(4)	
2624	168(17)	178(18)	187(19)	180(18)	163(16)	156(16)	145(15)	122(12)	82(8)			
2625	162(16)	169(17)	180(18)	171(17)	162(16)	155(16)	146(15)	123(12)	100(10)			
2721	325(32)	271(27)	291(29)	305(31)	267(27)	261(26)	212(21)	172(17)	168(17)	149(15)	134(13)	117(12)
2762	296(30)	345(35)	358(36)	338(34)	331(33)	345(34)	283(28)	234(23)	199(20)	191(19)	172(17)	181(18)
2864	565(56)	622(62)	643(64)	628(63)	620(62)	654(65)	609(61)	541(54)	469(47)	478(48)	482(48)	475(47)
2993	518(52)	600(60)	738(74)	829(83)	969(97)	1113(111)	1270(127)	1099(110)	1093(109)	955(96)	840(84)	719(72)
3118	273(27)	359(36)	441(44)	481(48)	557(56)	658(66)	753(75)	706(71)	733(73)	627(63)	513(51)	413(41)
3271	295(29)	300(30)	416(42)	416(42)	448(45)	516(52)	512(51)	510(51)	522(52)	419(42)	352(35)	280(28)
3393	189(19)	234(23)	267(27)	322(32)	348(35)	413(41)	472(47)	511(51)	447(45)	320(32)	305(30)	281(28)
3561	206(21)	283(28)	405(40)	556(56)	510(51)	634(63)	683(68)	711(71)	737(74)	630(63)	574(57)	566(57)
3706	423(42)	496(50)	674(67)	840(84)	754(75)	849(85)	854(85)	789(79)	838(84)	610(61)	516(52)	479(48)
3707	419(42)	487(49)	630(63)	785(78)	778(78)	824(82)	870(87)	792(79)	898(90)	621(62)	531(53)	530(53)
3807	360(36)	475(47)	568(57)	599(60)	726(73)	816(82)	805(80)	795(80)	793(79)	550(55)	526(53)	479(48)
3883	517(52)	545(55)	775(78)	818(82)	927(93)	949(95)	910(91)	727(73)	780(78)	724(72)	701(70)	775(77)
3985	482(48)	543(54)	629(63)	685(69)	682(68)	686(69)	638(64)	591(59)	669(67)	699(70)	803(80)	810(81)
4083	395(40)	535(54)	669(67)	609(61)	593(59)	629(63)	751(75)	649(65)	676(68)	769(77)	895(90)	1001(100)
4159	494(49)	538(54)	654(65)	705(70)	747(75)	940(94)	986(99)	856(86)	740(74)	780(78)	869(87)	1039(104)
4208	488(49)	525(52)	748(75)	933(93)	1023(102)	1269(127)	1191(119)	986(99)	749(75)	841(84)	957(96)	1175(118)
4263	963(96)	817(82)	1289(129)	1456(146)	1598(160)	1990(199)	1930(193)	1134(113)	1152(115)	1230(123)	1381(138)	1679(168)
4318	862(86)	1013(101)	1433(143)	1651(165)	1750(175)	1838(184)	1732(173)	1363(136)	1235(123)	1339(134)	1454(145)	1674(167)
4401	929(93)	976(98)	1348(135)	1500(150)	1430(143)	1482(148)	1378(138)	1341(134)	1202(120)	1645(164)	1678(168)	1729(173)
4510	959(96)	1089(109)	1539(154)	1817(182)	1702(170)	1712(171)	1544(154)	1398(140)	1572(157)	2053(205)	2008(201)	1722(172)
4630	590(59)	1061(106)	1831(183)	2048(205)	2150(215)	2279(228)	1868(187)	1516(152)	1362(136)	1970(197)	1948(195)	2006(201)
4709	409(41)	730(73)	1230(123)	1505(151)	1605(160)	1544(154)	1254(125)	1024(102)	1119(112)	1445(145)	1427(143)	1163(116)
4768	627(63)	682(68)	1239(124)	1462(146)	1388(139)	1394(139)	1117(112)	872(87)	1236(124)	1459(146)	1290(129)	1099(110)
4841	496(50)	533(53)	670(67)	795(80)	830(83)	842(84)	817(82)	705(70)	871(87)	840(84)	706(71)	573(57)
4905	534(53)	561(56)	644(64)	565(57)	687(69)	660(66)	692(69)	615(62)	717(72)	658(66)	613(61)	534(53)
4909		552(55)	755(75)	630(63)	659(66)	594(59)	693(69)	606(61)	766(77)	742(74)	676(68)	586(59)

measurements, whereas those of the present measurement are of the ground-state cross section only. Below $E_\alpha \approx 3.4$ MeV, the present measurements and those of Prior *et al.* [15] are in good agreement. At higher energies, the measurements slowly diverge because, below $E_\alpha \approx 3.4$ MeV, the ground-state cross section dominates the total cross section, whereas, at higher energies, the excited-state cross sections increase rapidly to become dominant. This is supported by the general trend of the differential cross-section measurements of Van der Zwan and Geiger [8] for the excited-state transitions, which show a rapid increase in the n_2 and n_3 cross sections above $E_\alpha \approx 3.4$ MeV. The data of Gibbons and Macklin [14] are considerably larger in cross sections than both the present data and that of Prior *et al.* [15] and show a different energy dependence.

V. THICK-TARGET YIELD COMPARISONS

The cross sections of this paper can be compared to thick-target yield measurements using the methods described in Roughton *et al.* [6], for example. The thick-target yield can be calculated for the cross-section σ and the stopping power cross-section $dE/dx(\rho x)$ by

$$Y(E) = \frac{N_A}{A_T}\int_0^E \frac{\sigma(E')}{dE/dx(\rho x)(E')}dE', \tag{2}$$

where E is the energy of the thick-target yield measurement and E' is the energy of the thin-target cross-section measurements. Stopping power cross sections and their uncertainties are taken from SRIM [28]. The uncertainties on the thick-target

TABLE II. Angular distribution coefficients [see Eq. (1)] for fits to center-of-mass differential cross sections for the ^{10}B(α, n_0) ^{13}N reaction for the present data combined with those of Van der Zwan and Geiger [8]. The energies are those of the incident beam energy (E_α). The number of degrees of freedom (ν) and the χ^2/ν of each fit are also given to indicate the quality of the fit. The uncertainty in the beam energy was ≈3 keV. The uncertainty in the angle-integrated cross section has significant contributions from the Legendre polynomial fitting of the differential cross section and for the normalization to the data of Van der Zwan and Geiger [8]. Angular distribution fits that included the data of Van der Zwan and Geiger [8] in addition to the present measurements are indicated by (*'s).

E_α	$\sigma_0 = 4\pi a_0$	a_1	a_2	a_3	a_4	a_5		
(keV)	(mb)			(mb/sr)			ν	χ^2/ν
1590	0.57(3)		−0.041(2)				7	0.83
1902	0.43(3)	−0.016(2)					8	0.42
2202	3.93(24)	−0.10(1)	−0.11(2)				8	0.29
2235	5.13(30)	−0.13(2)					10	0.77
2281	5.82(34)	−0.05(2)					9	1.07
2346	3.07(18)	0.02(1)					10	1.15
2509	1.14(7)	0.03(0)	−0.02(1)				8	0.73
2510	1.13(7)	0.03(0)	−0.02(1)				8	0.92
2624	1.49(10)	0.04(1)					7	2.92
2625	1.58(10)	0.02(1)					7	0.89
2721	2.59(15)	0.05(1)					13*	1.27
2762	3.15(18)	0.04(1)		−0.06(2)			9	0.46
2864	6.86(40)	−0.05(3)		−0.09(5)			9	0.19
2993	11.84(70)	−0.36(4)	−0.30(5)				9	0.45
3118	7.35(43)	−0.24(2)	−0.26(3)	0.14(3)			11*	0.93
3271	5.57(33)	−0.15(2)	−0.17(2)	0.13(3)	−0.11(3)		10*	0.94
3393	4.49(26)	−0.12(1)	−0.11(2)				12*	1.84
3560	7.31(42)	−0.32(2)	−0.16(2)				12*	0.40
3706	8.76(50)	−0.18(2)	−0.31(3)				12*	0.66
3707	8.45(49)	−0.19(2)	−0.29(3)				12*	0.66
3807	8.17(47)	−0.19(2)	−0.21(3)				12*	0.57
3883	9.45(54)	−0.26(3)		−0.21(4)			12*	0.92
3985	8.44(50)	−0.30(3)					10	1.17
4083	8.78(52)	−0.39(3)					10	1.92
4159	10.04(59)	−0.43(4)					10	1.49
4208	11.09(64)	−0.36(4)		−0.51(8)	0.35(7)		11*	0.61
4263	15.90(92)	−0.40(6)		−0.71(11)	0.28(10)		11*	2.18
4318	17.94(102)	−0.49(6)		−0.42(8)			12*	1.27
4400	17.61(101)	−0.68(7)	0.23(7)	−0.30(8)			11*	0.99
4510	19.64(112)	−0.66(7)		−0.36(8)			12*	1.10
4630	22.70(125)	−0.84(6)		−0.92(10)	−0.50(13)	0.54(9)	19*	0.82
4709	14.84(88)	−0.45(6)	−0.14(7)	−0.61(9)			8	1.65
4768	14.79(89)	−0.54(6)		−0.24(10)	−0.62(11)	0.36(8)	10*	1.75
4840	9.31(55)	−0.27(3)	−0.15(4)				9	1.17
4905	9.63(55)	−0.34(3)	−0.06(4)		−0.27(4)		11*	2.35
4909	8.37(48)	−0.33(2)			−0.33(2)		11*	0.77

yields are ≈8%, resulting for the uncertainties in the angle-integrated cross-section ≈6% and the stopping power ≈5%.

There are two thick-target yield measurements that have been presented in the literature, those of Bair and Gomez del Campo [7] and Roughton *et al.* [29]. Those of Roughton *et al.* [29] were made using the activation method. As stated earlier, this method is only sensitive to the ground-state transition of the ^{10}B(α, n) ^{13}N reaction since the excited states are all proton unbound. Bair and Gomez del Campo [7], on the other hand, measured the thick-target yield by the direct detection of neutrons, making their measurement sensitive to deexcitations for all final states. A comparison of the different thick-target yields is shown in Fig. 8. The large deviation of the two measurement methods is roughly consistent with the measurement of the total cross section versus only the ground-state component as discussed in Sec. IV for the thin-target cross-section measurements.

For comparison, the thick-target yields have also been calculated using the cross-section data of Prior *et al.* [15]. These thick-target yields can be directly comparable with those of Bair and Gomez del Campo [7] and show a larger yield. This may be because the yields of Bair and Gomez del Campo [7] are not corrected for the changing neutron efficiency at higher energies. The thick-target yields calculated from the present data are in good agreement with those measured directly by Roughton *et al.* [29].

VI. NIF SIMULATIONS

Coupled radiation-hydrodynamic simulations with an inline radiochemical network are a useful guide to reliably estimating the $^{10}\mathrm{B}(\alpha, n)\,^{13}\mathrm{N}$ production from a NIF implosion where a $^{10}\mathrm{B}$ dopant is present. Optimization of the $^{13}\mathrm{N}$ produced requires maximizing the α yield, but there are known complications prohibiting the naive choice of a DT-layered high-convergence implosion platform. The DT-layered high convergence experimental configuration has demonstrated neutron yields or, equivalently, α-particle yields slightly above 1.0×10^{16}. However, the presence of a dense DT-fuel layer adjacent to the remaining outer layer of the carbon ablator provides a large $^{13}\mathrm{N}$ signal on the order of 5.0×10^{9} atoms from the 14-MeV neutrons interacting with the deuterons in the fuel layer by the $^{12}\mathrm{C}(d, n)\,^{13}\mathrm{N}$ reaction. The analogous reaction $^{13}\mathrm{C}(p, n)\,^{13}\mathrm{N}$ does not appreciably contribute to a pure carbon ablator, whereas, a hydrocarbon ablator would supply scattered protons and a comparable signal.

Since this carbon-induced background would overwhelm the boron α-mediated reaction, a so-called "Symcap" platform was investigated instead. This particular capsule configuration replaces the DT-fuel layer with a hydrodynamically equivalent carbon ablator layer and, although not driven to high convergence, is capable of producing neutron yields of 3.0×10^{15} with DT-gas filling. Thus, a reduction of the background $^{13}\mathrm{N}$ signal might compensate for the lower neutron (α-particle) yield.

The relatively well-studied experimental configuration for NIF implosion N130813 was chosen as a basis for the simulation study. This experimental configuration was slightly modified by replacing the original pure deuterium gas fill with one of 1:1 DT and by introducing diborane (B_2H_6) gas as a dopant. Simulations were performed with two different energy-loss models: the default Maynard-Deutsch-Zimmerman model (MDZ) [30,31] and the Li-Petrasso-Zylstra model (LPZ) [32–34]. The addition of the dopant is expected to lower the neutron yield due to extra radiative loss at peak compression. The neutron yield for the modified configuration is 1.0×10^{15} when 1.1×10^{16} $^{10}\mathrm{B}$ atoms are added to the initial gas fill.

The results of these simulations are presented in Table III in which the main reactant products are listed for the two different energy-loss models using either the cross-section data presented here or that used previously in the HYDRA [35,36] simulation package, which is based on the measurements of Gibbons and Macklin [14]. As expected for the approximate factor of 5 discrepancy in the relevant energy range from $E_\alpha = 2.0$ to 3.5 MeV between the present measurements and those of Gibbons and Macklin [14] shown in Fig. 7, an experimentally discernible difference in $^{13}\mathrm{N}$ production is observed. For comparison, yields for the competing $^{10}\mathrm{B}(p, \alpha)\,^{7}\mathrm{Be}$ and $^{10}\mathrm{B}(p, \gamma)\,^{11}\mathrm{C}$ reactions are also given in Table III.

The bottom portion of the table also lists the total $^{13}\mathrm{N}$ background signal arising from either energetic deuterons or protons. Even though the α particle has a very short range in the compressed plasma, there is a 15% difference in the $^{13}\mathrm{N}$ production expected from the two models. Since the $^{13}\mathrm{N}$ production is inversely proportional to the energy loss, the LPZ model clearly predicts an enhanced α-particle energy loss. Broadly speaking, there is copious $^{13}\mathrm{N}$ production from the α-mediated reaction, but it is nearly equal to the $^{13}\mathrm{N}$ production from the competing deuteron and proton-mediated reactions. This competing signal remains a significant technical challenge to the extraction of the α-mediated contribution from the total signal. A different choice of ablator material, such as beryllium or high-purity aluminum, could suppress this undesirable background. The currently demonstrated neutron (α) yields for the beryllium platform are too small to produce appreciable $^{13}\mathrm{N}$. Aluminum capsules have not yet been tested with DT-fuel layers.

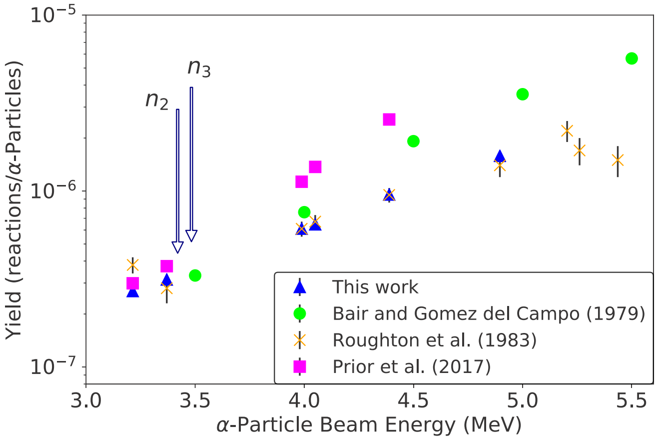

FIG. 8. Comparison of the thick-target yields measured by Roughton *et al.* [29] (orange stars) and Bair and Gomez del Campo [7] (green circles) with those calculated from the cross-section measurements of this paper (blue triangles) and that of Prior *et al.* [15] (pink squares). Note that the data of Roughton *et al.* [29] represent the thick-target yields from the ground-state transition of the $^{10}\mathrm{B}(\alpha, n_0)\,^{13}\mathrm{N}$ reaction, whereas those of Bair and Gomez del Campo [7] and those calculated from the cross-section data of Prior *et al.* [15] represent those from all transitions.

Finally, a qualitative estimate may be derived as a consistency check on the α-mediated production. The number of $^{13}\mathrm{N}$ atoms P is the integral of the α-particle flux $f_\alpha(E, t)$, multiplied by the number of loaded $^{10}\mathrm{B}$ atoms n_B and the reaction cross-section $\sigma(E)$ over energy and time,

$$P = \iint dt\, dE\, f_\alpha(E, t) n_\mathrm{B} \sigma(E). \qquad (3)$$

Approximating the α-particle flux by

$$f_\alpha(E, t) \approx f_\alpha(E)_\mathrm{ave} \delta(E - E_\alpha)/\tau_\mathrm{burn}, \qquad (4)$$

where $f_\alpha(E)_\mathrm{ave}/\tau_\mathrm{burn}$ is the burn-averaged flux and the α particles are assumed to be monoenergetic with energy $E_\alpha =$ 3.45 MeV leads to the approximation,

$$P \approx f_\alpha(E_\alpha)_\mathrm{ave} n_\mathrm{B} \sigma(E_\alpha). \qquad (5)$$

From the simulations $f_\alpha(E)_\mathrm{ave} \approx 1.2 \times 10^{19}$ α particles with an assumed dopant loading of 1.0×10^{16} $^{10}\mathrm{B}$ atoms and $\sigma(E_\alpha) \approx 1.0 \times 10^{-26}\,\mathrm{cm}^2$ provide an estimate of $1.2 \times 10^{8}\,^{13}\mathrm{N}$ atoms, which compares favorably with the more accurate values obtained from the simulations.

TABLE III. Comparison of simulated NIF radioactive reactant products. The top portion of the table lists the main radioactive reactant products for simulations using the MDZ and LPZ energy-loss models with both the ^{10}B$(\alpha, n)^{13}$N cross section of the present paper and that of Gibbons and Macklin [14]. The bottom portion summarizes the background production of ^{13}N for the ^{12}C$(d, n)^{13}$N and ^{13}C$(p, n)^{13}$N reactions. The total value of ^{13}N from the background reactions is similar to that produced from the ^{10}B$(\alpha, n)^{13}$N reaction. Yields for the competing ^{10}B$(p, \alpha)^{7}$Be and ^{10}B$(p, \gamma)^{11}$C reactions are also given.

Model	^{10}B$(\alpha, n)^{13}$N	^{10}B$(p, \alpha)^{7}$Be	^{10}B$(p, \gamma)^{11}$C
Present paper			
MDZ	8.2×10^7	4.3×10^7	2.6×10^7
LPZ	7.0×10^7	4.1×10^7	2.4×10^7
Gibbons and Macklin [14]			
MDZ	5.8×10^8	4.3×10^7	2.6×10^7
LPZ	4.9×10^8	4.0×10^7	2.4×10^7
Competing reactions			
	^{13}N background	^{12}C$(d, n)^{13}$N	^{13}C$(p, n)^{13}$N
MDZ	8.6×10^8	8.3×10^8	3.8×10^7
LPZ	7.5×10^8	7.1×10^8	4.2×10^7

VII. CONCLUSIONS

New measurements of the ^{10}B$(\alpha, n_0)^{13}$N reaction have been made over the energy range applicable to calculate the ^{13}N production under the typical temperature conditions of a NIF shot. By performing neutron spectroscopy with better than 0.5-MeV energy resolution, the ground-state portion of the cross section, which is the sole component that produces ^{13}N, was separated from the excited states, and the angle-integrated cross section was obtained for the first time. The present results show large deviations from the cross sections of Gibbons and Macklin [14], which were previously adopted in the HYDRA code for simulating ^{13}N yields from this reaction in a NIF implosion. By performing a preliminary NIF fuel shot and dopant yield calculations, it has been demonstrated that the present measurements result in an ≈85% reduction in the predicted ^{13}N yield from ^{10}B$(\alpha, n_0)^{13}$N. Furthermore, the improved uncertainty in the cross section of the present measurements increases the accuracy of this estimate. This demonstrates a clear need for an improvement in the accuracy of the cross-section data used in NIF simulations.

To demonstrate the effect of the revised cross section for the ^{10}B$(\alpha, n_0)^{13}$N reaction, simulations of the production of ^{13}N from the ^{12}C$(d, n)^{13}$N and ^{13}C$(p, n)^{13}$N reactions have been performed. These predict that only about 10% of the total production of ^{13}N will be from the ^{10}B$(\alpha, n)^{13}$N reaction. Since a subtraction of the ^{13}N background yields must be performed, this significantly increases the uncertainty in the ^{13}N production from the ^{10}B$(\alpha, n)^{13}$N reaction when traditional carbon capsules are used. However, a different capsule material, perhaps beryllium or aluminum, could be utilized, which would dramatically decrease the yields from the ^{12}C$(d, n)^{13}$N and ^{13}C$(p, n)^{13}$N background reactions, but improved neutron yields for one of these alternate capsule types must first be achieved.

ACKNOWLEDGMENTS

This research utilized resources from the Notre Dame Center for Research Computing and was supported by the National Science Foundation through Grants No. PHY-1713857 and No. NSF-PHY-1404218 (Rutgers) and the Joint Institute for Nuclear Astrophysics through Grants No. PHY-0822648 and No. PHY-1430152 (JINA Center for the Evolution of the Elements). This material was based upon work supported by the US Department of Energy, Office of Science, Office of Nuclear Physics, under Award No. DE-AC05-00OR22725. Also supported, in part, by the US Department of Energy National Nuclear Security Administration Stewardship Science Academic Alliances under cooperative Agreement No. DE-NA0002132 (Rutgers). Research at LLNL is performed under the auspices of Lawrence Livermore National Security, LLC, Contract No. DE-AC52-07NA27344. The authors would like to thank the NIST Center for Neutron Research for their technical support. Partial funding for this research was provided by the U.S. National Research Council. Trade names and commercial products are identified in this paper to specify the experimental procedures in adequate detail. This identification does not imply recommendation or endorsement by the authors or by the National Institute of Standards and Technology, nor does it imply that the products identified are necessarily the best available for the purpose. Contributions of the National Institute of Standards and Technology are not subject to copyright.

---

[1] E. I. Moses, R. N. Boyd, B. A. Remington, C. J. Keane, and R. Al-Ayat, Phys. Plasmas **16**, 041006 (2009).

[2] O. A. Hurricane and M. C. Herrmann, Annu. Rev. Nucl. Part. Sci. **67**, 213 (2017).

[3] C. J. Cerjan, L. Bernstein, L. B. Hopkins, R. M. Bionta, D. L. Bleuel, J. A. Caggiano, W. S. Cassata, C. R. Brune, D. Fittinghoff, J. Frenje, M. Gatu-Johnson, N. Gharibyan, G. Grim, C. Hagmann, A. Hamza, R. Hatarik, E. P. Hartouni,

E. A. Henry, H. Herrmann, N. Izumi, D. H. Kalantar, H. Y. Khater, Y. Kim, A. Kritcher, Y. A. Litvinov, F. Merrill, K. Moody, P. Neumayer, A. Ratkiewicz, H. G. Rinderknecht, D. Sayre, D. Shaughnessy, B. Spears, W. Stoeffl, R. Tommasini, C. Yeamans, C. Velsko, M. Wiescher, M. Couder, A. Zylstra, and D. Schneider, J. Phys. G: Nucl. Part. Phys. **45**, 033003 (2018).

[4] F. Ajzenberg-Selove, Nucl. Phys. A **523**, 1 (1991).

[5] D. A. Shaughnessy, C. A. Velsko, D. R. Jedlovec, C. B. Yeamans, K. J. Moody, E. Tereshatov, W. Stoeffl, and A. Riddle, Rev. Sci. Instrum. **83**, 10D917 (2012).

[6] N. A. Roughton, M. R. Fritts, R. J. Peterson, C. S. Zaidins, and C. J. Hansen, At. Data Nucl. Data Tables **23**, 177 (1979).

[7] J. K. Bair and J. Gomez del Campo, Nucl. Sci. Eng. **71**, 18 (1979).

[8] L. Van der Zwan and K. W. Geiger, Nucl. Phys. A **216**, 188 (1973).

[9] I. Curie and M. F. Joliot, Compt. R. **198**, 254 (1934).

[10] J. Chadwick, Proc. R. Soc. London, Ser. A **142**, 1 (1933).

[11] I. Curie and F. Joliot, Nature (London) **133**, 721 (1934).

[12] T. W. Bonner, A. A. Kraus, J. B. Marion, and J. P. Schiffer, Phys. Rev. **102**, 1348 (1956).

[13] R. L. Walker, Phys. Rev. **76**, 244 (1949).

[14] J. H. Gibbons and R. L. Macklin, Phys. Rev. **114**, 571 (1959).

[15] R. M. Prior, M. C. Spraker, R. H. France, S. Stave, M. W. Ahmed, H. J. Karwowski, J. M. Mueller, L. S. Myers, and H. R. Weller, Nucl. Sci. Tech. **28**, 106 (2017).

[16] M. Febbraro, C. C. Lawrence, H. Zhu, B. Pierson, R. O. Torres-Isea, F. D. Becchetti, J. J. Kolata, and J. Riggins, Nucl. Instrum. Methods Phys. Res., Sect. A **784**, 184 (2015).

[17] C. C. Lawrence, A. Enqvist, M. Flaska, S. A. Pozzi, and F. D. Becchetti, Nucl. Instrum. Methods Phys. Res., Sect. A **729**, 924 (2013).

[18] F. D. Becchetti, R. S. Raymond, R. O. Torres-Isea, A. Di Fulvio, S. D. Clarke, S. A. Pozzi, and M. Febbraro, Nucl. Instrum. Methods Phys. Res., Sect. A **820**, 112 (2016).

[19] R. G. Downing, G. P. Lamaze, J. K. Langland, and S. T. Hwang, J. Res. Natl. Inst. Stand. Technol. **98**, 109 (1993).

[20] G. P. Lamaze, H. Chen-Mayer, J. K. Langland, and R. G. Downing, Surf. Interface Anal. **25**, 217 (1997).

[21] See Supplemental Material at http://link.aps.org/supplemental/10.1103/PhysRevC.100.034601 for details.

[22] W. J. Huang, G. Audi, M. Wang, F. G. Kondev, S. Naimi, and X. Xu, Chin. Phys. C **41**, 030002 (2017).

[23] M. Wang, G. Audi, F. G. Kondev, W. J. Huang, S. Naimi, and X. Xu, Chin. Phys. C **41**, 030003 (2017).

[24] T. N. Massey, D. K. Jacobs, S. I. Al-Quraishi, S. M. Grimes, C. E. Brient, W. B. Howard, and J. C. Yanch, J. Nucl. Sci. Technol. **39**, 677 (2002).

[25] M. Febbraro, R. Toomey, S. Pain, K. Chipps, B. Becker, R. Newby, Z. Meisel, T. Massey, C. Brune, Q. Liu, R. deBoer, K. Macon, A. Boeltzig, J. O'Neill, M. Smith, M. Wiescher, D. Soltesz, I. Sultana, K. Brandenburg, S. Subendi, S. Paneru, T. Danely, and Y. Alberty-Jones, "The ORNL Deuterated Spectroscopic Array - ODeSA" (unpublished).

[26] S. A. Pozzi, E. Padovani, and M. Marseguerra, Nucl. Instrum. Methods Phys. Res., Sect. A **513**, 550 (2003).

[27] J. L. Tain and D. Cano-Ott, Nucl. Instrum. Methods Phys. Res., Sect. A **571**, 728 (2007).

[28] J. F. Ziegler, M. D. Ziegler, and J. P. Biersack, Nucl. Instrum. Methods Phys. Res., Sect. B **268**, 1818 (2010).

[29] N. A. Roughton, T. P. Intrator, R. J. Peterson, C. S. Zaidins, and C. J. Hansen, At. Data Nucl. Data Tables **28**, 341 (1983).

[30] G. Maynard and C. Deutsch, J. Phys. France **46**, 1113 (1985).

[31] G. B. Zimmerman, in *The 13th International Conference on Laser Interactions and Related Plasma Phenomena*, edited by G. H. Miley and E. M. Campbell, AIP Conf. Proc. No. 406 (AIP, New York, 1997), p. 23.

[32] C.-K. Li and R. D. Petrasso, Phys. Rev. Lett. **70**, 3059 (1993).

[33] C.-K. Li and R. D. Petrasso, Phys. Rev. Lett. **114**, 199901(E) (2015).

[34] A. B. Zylstra, Using fusion-product spectroscopy to study inertial fusion implosions, stopping power, and astrophysical nucleosynthesis at OMEGA and the NIF, Ph.D. thesis, Massachusetts Institute of Technology, 2015.

[35] M. M. Marinak, G. D. Kerbel, N. A. Gentile, O. Jones, D. Munro, S. Pollaine, T. R. Dittrich, and S. W. Haan, Phys. Plasmas **8**, 2275 (2001).

[36] M. M. Marinak, S. W. Haan, T. R. Dittrich, R. E. Tipton, and G. B. Zimmerman, Phys. Plasmas **5**, 1125 (1998).